Simulation of Spontaneous Ca^{2+} Oscillations in Astrocytes Mediated by Voltage-Gated Calcium Channels

Shuai Zeng, Bing Li, Shaoqun Zeng, and Shangbin Chen*
Britton Chance Center of Biomedical Photonics, Wuhan National Laboratory for Optoelectronics–Huazhong University of Science and Technology, Wuhan, China

ABSTRACT The purpose of this computational study was to investigate the possible role of voltage-gated Ca^{2+} channels in spontaneous Ca^{2+} oscillations of astrocytes. By incorporating different types of voltage-gated Ca^{2+} channels and a previous model, this study reproduced typical Ca^{2+} oscillations in silico. Our model could mimic the oscillatory phenomenon under a wide range of experimental conditions, including resting membrane potential (−75 to −60 mV), extracellular Ca^{2+} concentration (0.1 to 1500 μM), temperature (20 to 37°C), and blocking specific Ca^{2+} channels. By varying the experimental conditions, the amplitude and duration of Ca^{2+} oscillations changed slightly (both <25%), while the frequency changed significantly (~400%). This indicates that spontaneous Ca^{2+} oscillations in astrocytes might be an all-or-none process, which might be frequency-encoded in signaling. Moreover, the properties of Ca^{2+} oscillations were found to be related to the dynamics of Ca^{2+} influx, and not only to a constant influx. Therefore, calcium channels dynamics should be used in studying Ca^{2+} oscillations. This work provides a platform to explore the still unclear mechanism of spontaneous Ca^{2+} oscillations in astrocytes.

INTRODUCTION

Astrocytes are probably the most diverse population of glial cells (1). Twenty years ago, astrocytes were merely thought to function as passive histological support elements in the nervous system (2). Recent groundbreaking studies of astrocytes have suggested that these cells have a more active and direct role in the dynamic regulation of cerebral microcirculation (3–5), neuronal production (6–8), synaptic transmission (9,10), neuronal activation (11), and specific neurological diseases (12–15). Spontaneous astrocytic Ca^{2+} oscillations have been observed and implicated in important functions of the brain (11,16–18). However, the mechanism of spontaneous Ca^{2+} oscillations is still unclear. Therefore, it is critical to understand how the Ca^{2+} oscillations are generated and modulated.

Many experimental results suggested that an inositol 1,4,5-triphosphate (IP_3) dependent calcium-induced calcium release (CICR) mechanism is involved in Ca^{2+} oscillations (16,18,19). This was central to the process in the intracellular space (ICS). In fact, the Ca^{2+} oscillations needed both extracellular and intracellular Ca^{2+} contribution (17). Voltage-gated calcium channels (VGCCs) were found to be involved in Ca^{2+} oscillations in pharmacological trials (11,16,17,20). The putative notion of Ca^{2+} oscillations in astrocytes was that a small influx of Ca^{2+} into the cytoplasm via VGCCs induces CICR activated by IP_3 (21–23). Several models have been previously developed to describe Ca^{2+} oscillations in the cytoplasm (24–27). In Lavrentovich and Hemkin's (LH) work, a mathematical model was successfully employed to simulate the IP_3-dependent CICR process (26). The initiation of Ca^{2+} oscillations was hypothesized to be due to a small and constant influx of calcium ions through the membrane. The model showed qualitative consistency with experiments (11,16,17). However, the pathway of Ca^{2+} influx was not clarified. To the best of our knowledge, no model has taken VGCCs into account during the spontaneous Ca^{2+} oscillations in astrocytes. Here we expand the LH model by combining it with different types of VGCCs. The electrophysiological properties of these VGCCs were described by the Hodgkin-Huxley (HH) equations (28). Since the Ca^{2+} influx would be mediated by physiologically relevant conditions (membrane potential, extracellular Ca^{2+} concentration, temperature, and blocking of specific channels), in this study, a variable but tractable Ca^{2+} influx replaced a constant flow. The Ca^{2+} oscillations dynamics (including the onset, frequency, half-maximal duration, and amplitude) in the physiologically relevant range were analyzed. The simulation results reasonably mimicked the experimental observations of spontaneous Ca^{2+} oscillations in astrocytes.

METHODS

The HH equation and the LH model were combined: Ca^{2+} influx via VGCCs induces IP_3-activated CICR and cytosol Ca^{2+} oscillations. Three compartments were considered, including the extracellular space (ECS), intracellular space (ICS), and the intraspace of endoplasmic reticulum (ER). Three variables (Ca^{2+} concentration in ICS and ER, and IP_3 concentration in ICS) were mainly modeled in this study.

Voltage-gated calcium channels

The astrocyte is separated from the ECS by the membrane, with two compartments representing ECS and ICS. The different types of VGCCs are distributed in the cellular membrane and form the pathway of calcium ions influx (Fig. 1). According to physiological and pharmacological properties, VGCCs are classified as low-voltage-activated channels (T-type) and

Submitted December 7, 2008, and accepted for publication August 11, 2009.

*Correspondence: sbchen@mail.hust.edu.cn

Editor: Edward H. Egelman.

0006-3495/09/11/2429/9 $2.00

doi: 10.1016/j.bpj.2009.08.030

several types of high-voltage-activated channels (L-, N-, P-, Q-, and R-types) (1,29). Previous studies showed that the electrophysiological properties in astrocytes resemble those of corresponding VGCCs in neurons (1,29,30). For simplicity, in this model, the P-, Q-, and R-types were grouped together as one type represented by the R-type. Thus, four HH equations were used to model the VGCCs with the same formula, but with modified conductance parameters from the work of Amini et al. (31). The four new parameters (Table 1) were smaller than those in Amini et al. (31) and were determined by the method of trial-and-error. Based on electrophysiological data (30), in this work, the T-type conductance was the smallest.

The four types of currents were presented as the T-type calcium channel current ($I_{Ca,T}$), L-type current ($I_{Ca,L}$), N-type current ($I_{Ca,N}$), and the residual high-voltage-activated calcium channel current ($I_{Ca,R}$), which stands for the current combination of R-, P-, and Q-types. All the four types of Ca^{2+} ionic currents through VGCCs shared the generalized HH form (28):

$$I = gm^p h^q (V - E_{Ca}). \quad (1)$$

Here, g is the membrane conductance. The values m and h represent channel activation and inactivation, and p and q are integers that are prespecified and fixed for each type of channel (both are "1" in our model). The values m and h relax exponentially to their steady-state values $\overline{m}$ and $\overline{h}$ according to

$$\frac{dm}{dt} = \frac{\overline{m} - m}{\tau_m}, \quad \frac{dh}{dt} = \frac{\overline{h} - h}{\tau_h}. \quad (2)$$

V is the membrane potential, and E_{Ca} is the Nernst potential for Ca^{2+} ion:

$$E_{Ca} = \frac{RT}{zF} \ln \frac{Ca_{out}}{Ca_{Cyt}}. \quad (3)$$

In Eq. 3, R is the ideal gas constant, T is the temperature, z is the valence of Ca^{2+} ion, and F is the Faraday constant. The concrete formula for every type of calcium current is given in detail in Table 2. The steady-state activation fraction of different channels versus membrane potential is shown in Fig. 2. Since the period of spontaneous Ca^{2+} oscillations in astrocytes was reported to be ~100 s (11,14), the steady-state current of VGCCs was considered here. The total of calcium current flow through VGCCs in an individual cell can be calculated as

$$I_{VGCC} = I_{Ca,T} + I_{Ca,L} + I_{Ca,N} + I_{Ca,R}. \quad (4)$$

In Eq. 4, the entry of calcium current into an astrocyte was defined as negative. To calculate the current contribution to the increase of Ca^{2+} concentration, the current was converted into the flux as

$$J_{VGCC} = -\frac{I_{VGCC}}{zFV_{ast}}. \quad (5)$$

V_{ast} is the volume of an astrocyte assumed as a spherical soma with a radius of 5 μm, calculated to be 5.233×10^{-13} l. J_{VGCC} is the change rate of Ca^{2+} concentration with the unit μM/s. In this way, not only the total Ca^{2+} flux but also every subpopulation influx via different VGCCs could be recorded.

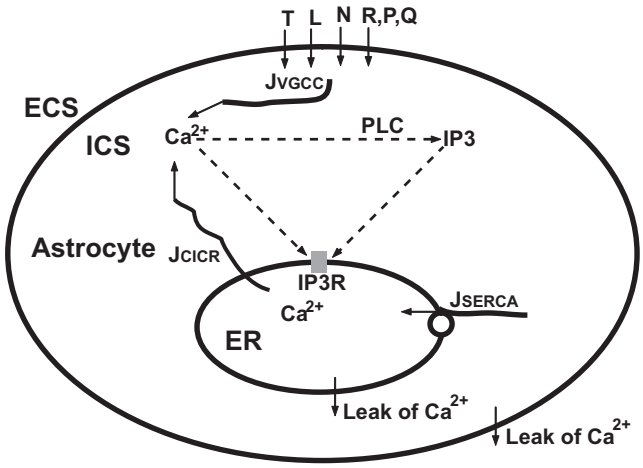

FIGURE 1 Schematic drawing of voltage-gated calcium channels (VGCCs) mediating Ca^{2+} oscillations. The main features within the astrocyte were referred to in Lavrentovich and Hemkin's model (26). Different VGCCs (T, L, N, R, P, and Q) form Ca^{2+} influx J_{VGCC} from the extracellular space (ECS) to the intracellular space (ICS). Cytoplasmic Ca^{2+} enhances the production of inositol 1,4,5-triphosphate (IP_3) catalyzed by phospholipase C (PLC). Cytoplasmic Ca^{2+} and IP_3 mediate IP_3 receptors (IP_3R), inducing Ca^{2+} flow J_{CICR} out of the endoplasmic reticulum (ER). J_{SERCA} represents ER Ca^{2+} filling by the sarcoplasmic/endoplasmic reticulum calcium ATPase (SERCA). Two "leak" arrows indicate the leak flux due to the concentration gradient.

Calcium-induced calcium release

Some of the previous works showed that astrocytes exhibited Ca^{2+} oscillations via an IP_3-dependent CICR mechanism (16,19,23,25). The recent LH model (26) of this phenomenon was adopted in this study. In the LH model, ER was considered as the calcium store. There were three main variables: Ca^{2+} concentration in the cytosol (Ca_{Cyt}); Ca^{2+} concentration in the ER (Ca_{ER}); and the IP_3 concentration in the cell (IP_{Cyt}). Each variable was described by an ordinary differential equation (Eqs. 6–8):

$$\frac{dCa_{Cyt}}{dt} = J_{VGCC} - P_{out}Ca_{Cyt} + J_{CICR} + J_{SERCA} + P_f(Ca_{ER} - Ca_{Cyt}). \quad (6)$$

Here J_{VGCC} is the same variable as in Eq. 5. $P_{out}Ca_{Cyt}$ represents the rate of calcium efflux from the cytosol into the extracellular space. J_{CICR} represents the IP_3-mediated CICR flux to the cytosol from the ER. J_{SERCA} is the flux from the sarcoplasmic/endoplasmic reticulum calcium ATPase (SERCA), which fills the ER with calcium ions from the cytosol. $P_f(Ca_{ER}–Ca_{Cyt})$ describes the leakage flux from the ER into the cytosol along the concentration gradient:

$$\frac{dCa_{ER}}{dt} = J_{SERCA} - J_{CICR} + P_f(Ca_{ER} - Ca_{Cyt}). \quad (7)$$

In Eq. 7, all three terms on the right-hand side have the same meaning as in Eq. 6.

$$\frac{dIP_{Cyt}}{dt} = J_{PLC} - P_{deg}IP_{Cyt}. \quad (8)$$

In Eq. 8, J_{PLC} denotes IP_3 production, and $P_{deg}IP_{Cyt}$ represents IP_3 degradation. In the above three equations, P_{out}, P_f, and P_{deg} are constants, whereas the other three terms J_{CICR}, J_{SERCA}, and J_{PLC} are determined by the following three equations:

$$J_{CICR} = \frac{4M_{CICR}P_{CaA}^{n1}Ca_{Cyt}^{n1}IP_{Cyt}^{n2}(Ca_{ER} - Ca_{Cyt})}{(Ca_{Cyt}^{n1} + P_{CaA}^{n1})(Ca_{Cyt}^{n1} + P_{CaI}^{n1})(IP_{Cyt}^{n2} + P_{IP3}^{n2})}, \quad (9)$$

$$J_{SERCA} = M_{SERCA}Ca_{Cyt}^2/(Ca_{Cyt}^2 + P_{SERCA}^2), \quad (10)$$

$$J_{PLC} = M_{PLC}Ca_{Cyt}^2/(Ca_{Cyt}^2 + P_{PCa}^2). \quad (11)$$

TABLE 1 Variables and parameters used in the model

Symbol	Equation*	Description	Value (unit)
I	Eq. 1	Ionic current	fA
g	Eq. 1	Membrane conductance	μS
m	Eq. 1	Channel activation variable	—
h	Eq. 1	Channel inactivation variable	—
V	Eq. 1	Membrane potential	mV
E_{Ca}	Eq. 1	Nernst potential of Ca^{2+}	mV
p	Eq. 1	Integer for activation variable	1
q	Eq. 1	Integer for inactivation variable	1
t	Eq. 2	Time	s
z	Eq. 3	Valence of Ca^{2+} ion	2
T	Eq. 3	Temperature	300 K
R	Eq. 3	Ideal gas constant	8.31 J/(mole·K)
F	Eq. 3	Faraday's constant	96,485 Coul/mole
$\overline{g}_T$	Table 2	Steady conductance of T-type channel	0.0600 pS
$\overline{g}_L$	Table 2	Steady conductance of L-type channel	3.5000 pS
$\overline{g}_N$	Table 2	Steady conductance of N-type channel	0.3900 pS
$\overline{g}_R$	Table 2	Steady conductance of R-type channel	0.2225 pS
I_{VGCC}	Eq. 4	Total Ca^{2+} current through all VGCCs	fA
V_{ast}	Eq. 5	Volume of an astrocyte	5.233×10^{-13} l
J_{VGCC}	Eq. 5	Influx of extracellular Ca^{2+} into cytosol via VGCCs	0 μM/s ($t = 0$)
Ca_{Cyt}	Eq. 6	Ca^{2+} concentration in cytosol	0.1 μM ($t = 0$)
J_{CICR}	Eq. 6	IP_3-mediated CICR flux to the cytosol from the ER	0 μM/s ($t = 0$)
J_{SERCA}	Eq. 6	The filling with Ca^{2+} from the cytosol to ER	0 μM/s ($t = 0$)
P_{out}	Eq. 6	Rate of calcium efflux from the cytosol into ECS	0.5 s^{-1}
P_f	Eq. 6	Rate of leak flux from the ER into the cytosol	0.5 s^{-1}
Ca_{ER}	Eq. 6	Ca^{2+} concentration in ER	1.5 μM ($t = 0$)
IP_{Cyt}	Eq. 8	IP_3 concentration in cytosol	0.1 μM ($t = 0$)
J_{PLC}	Eq. 8	Production of IP_3	0 μM/s ($t = 0$)
P_{deg}	Eq. 8	Rate of IP_3 degradation	0.08 s^{-1}
M_{CICR}	Eq. 9	Maximum flux of calcium ions into the cytosol	40 s^{-1}
P_{CaA}	Eq. 9	Activating affinity	0.15 μM
P_{CaI}	Eq. 9	Inhibiting affinity	0.15 μM
$n1$	Eq. 9	Hill coefficient	2.02
$n2$	Eq. 9	Hill coefficient	2.2
P_{IP3}	Eq. 9	Half-saturation constant for IP_3 activation of IP_3R	0.1 μM
M_{SERCA}	Eq. 10	Maximum flux across SERCA	15.0 μM/s
P_{SERCA}	Eq. 10	Half-saturation constant for SERCA activation	0.1 μM
M_{PLC}	Eq. 11	Maximum production rate of PLC	0.05 μM/s
P_{PCa}	Eq. 11	Half-saturation constant for calcium activation of PLC	0.3 μM

*Equations indicate the variables and parameters that are appearing for the first time.

Among them, M_{CICR}, M_{SERCA}, M_{PLC}, P_{CaA}, P_{CaI}, P_{IP3}, P_{SERCA}, P_{PCa}, $n1$, and $n2$ are all constants. All the variables and parameters used in the model are listed in Table 1. The majority of the parameters were the same as in the LH model (26). For some variables, the initial values are indicated as $t = 0$ in Table 1.

Implementation

All the computations and visualizations of the model were implemented in the MATLAB environment (MATLAB7.0,The MathWorks, Natick, MA). The model system was discretized with a temporal precision of 10 ms. The canonical explicit difference method was used to solve the three ordinary differential equations (Eqs. 6–8). All the variables in the model were calculated and recorded with double precision. A specific script for the model was constructed (supplied in the Supporting Material). Five parameters (the onset, frequency, period, half-maximal duration, and amplitude) were used to describe the properties of Ca^{2+} oscillations. The onset value was calculated as the time from the initiation of simulation to the first peak time-point of Ca^{2+} oscillations. The other four parameters were routinely defined as the same as in the oscillations phenomena (32), and the half-maximal duration was labeled "duration" in Tables 3 and 4.

RESULTS

Typical properties of Ca^{2+} oscillations

Our model successfully reproduced Ca^{2+} oscillations in astrocytes. Parameter values were fixed as in Table 1 for all simulations unless otherwise noted. Fig. 3 shows the results with a time duration of 800 s, a membrane potential of −65 mV, and ECS Ca^{2+} concentration of 1.5 mM. In ICS, five Ca^{2+} oscillation episodes occurred in a train with the amplitude of 0.66 μM and the period of 139.5 s. In ER, the Ca^{2+} oscillations showed a much larger amplitude of 4.87 μM, but the same period. Accompanying the Ca^{2+} oscillations, the concentration of IP_3 also oscillated with the same period. In

TABLE 2 Details of the voltage-gated calcium channels

Channel type	Equation of channel kinetics
T-type	$I_{Ca,T} = \bar{g}_T m_T (h_{Tf} + 0.04 h_{Ts})(V - E_{Ca})$
	$\bar{m}_T = \frac{1.0}{1.0 + e^{-(V+63.5)/1.5}}$ $\bar{h}_T = \frac{1.0}{1.0 + e^{(V+76.2)/3.0}}$
	$\tau_{h_{Tf}} = 50.0e^{-((V+72.0)/10.0)^2} + 10.0$
	$\tau_{h_{Ts}} = 400.0e^{-((V+100.0)/10.0)^2} + 400.0$
	$\tau_{m_T} = 65.0e^{-((V+68.0)/6.0)^2} + 12.0$
L-type	$I_{Ca,L} = \bar{g}_L m_L h_L (V - E_{Ca})$
	$\bar{m}_L = \frac{1.0}{1.0 + e^{-(V+50.0)/3.0}}$ $h_L = \frac{0.00045}{0.00045 + Ca_{cyt}}$
	$\tau_{m_L} = 18.0e^{-((V+45.0)/20.0)^2} + 1.5$
N-type	$I_{Ca,N} = \bar{g}_N m_N h_N (V - E_{Ca})$
	$\bar{m}_N = \frac{1.0}{1.0 + e^{-(V+45.0)/7.0}}$
	$h_N = \frac{0.00010}{0.00010 + Ca_{cyt}}$
	$\tau_{m_N} = 18.0e^{-((V+70.0)/25.0)^2} + 0.30$
R-type	$I_{Ca,R} = \bar{g}_R m_R h_R (V - E_{Ca})$
	$\bar{m}_R = \frac{1.0}{1.0 + e^{-(V+10.0)/10.0}}$ $\bar{h}_R = \frac{1.0}{1.0 + e^{(V+48.0)/5.0}}$
	$\tau_{m_R} = 0.1e^{-((V+62.0)/13.0)^2} + 0.05$
	$\tau_{h_R} = 0.5e^{-((V+55.6)/18.0)^2} + 0.5$

the enlarged plot from the second period of Ca^{2+} oscillations (Fig. 4), the three variables showed different peak time-points, the ER Ca^{2+} oscillations preceded cytoplasmic Ca^{2+} oscillations by 5.8 s, and cytoplasmic Ca^{2+} oscillations were followed by IP_3 oscillations with a time-lag of 12.4 s.

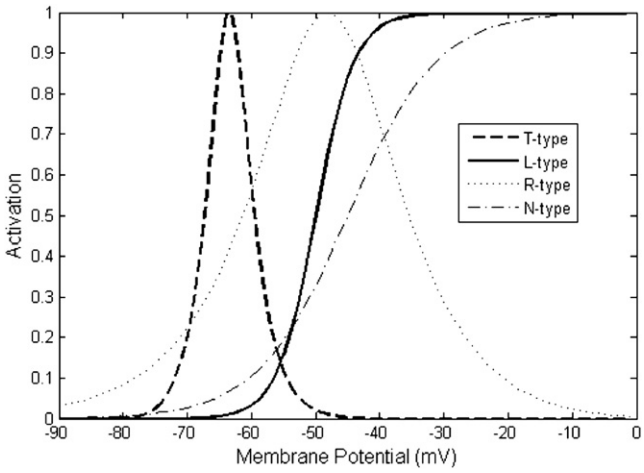

FIGURE 2 Steady-state activation fraction of different voltage-gated calcium channels. The activation fraction is the normalized product of the activation and inactivation variables m and h from every type of channel. The cytoplasmic Ca^{2+} concentration was fixed at 0.1 μM for considering the Ca^{2+} concentration dependence.

TABLE 3 Properties of Ca^{2+} oscillations under different membrane potentials

Potential (mV)	Amplitude (μM)	Period (s)	Frequency (Hz)	Onset (s)	Duration (s)
−70	0.5276	528.1	0.0019	517.2	13.51
−69	0.5726	301.6	0.0033	289.5	13.87
−68	0.5977	222.5	0.0045	209.8	14.15
−67	0.6211	177.5	0.0056	164.1	14.47
−66	0.6438	150.2	0.0067	136.1	14.84
−65	0.6614	139.5	0.0072	125.0	15.26

The sequential oscillation order of ER Ca^{2+}, cytoplasmic Ca^{2+}, and IP_3 was consistent with previous works (21–23,33).

Dependence of Ca^{2+} oscillations on membrane potential

Among the resting membrane potentials (−75 to −60 mV) (1), a narrow range of potential (−70.0 to −64.9 mV) was validated with Ca^{2+} oscillations at ECS Ca^{2+} concentration of 1.5 mM. Different manifestations of Ca^{2+} oscillations under different potentials were found (Fig. 5). The frequency of Ca^{2+} oscillations strongly depended on membrane potential. The bifurcation diagram is shown in Fig. 6 *A*. When the membrane potential was <-70.0 mV or >-64.9 mV, there was no Ca^{2+} oscillation. In the oscillatory potential range, the amplitude of Ca^{2+} oscillations changed slightly, but the frequency varied dramatically (Fig. 6 *B*). The properties of Ca^{2+} oscillations under different membrane potentials are summarized in Table 3. The period of Ca^{2+} oscillation was ~139.5 to 528.1 s, and the frequency was ~0.0019 to 0.0072 Hz. The amplitude of Ca^{2+} oscillation was ~0.5276 to 0.6614 μM. The half-maximal duration of Ca^{2+} oscillations was ~13.51 to 15.26 s.

Dependence of Ca^{2+} oscillations on extracellular Ca^{2+} concentration

The spontaneous Ca^{2+} oscillations were found to be related to extracellular Ca^{2+} concentration (Fig. 7). During the simulation, the membrane potential was fixed at −65 mV. When the extracellular Ca^{2+} concentration varied from 0.1 μM to 1.5 mM, the frequency of Ca^{2+} oscillations markedly increased. If the extracellular Ca^{2+} concentration was >3.0 mM, the Ca^{2+} oscillations would disappear. The parameters of Ca^{2+} oscillations dynamics under different extracellular Ca^{2+} concentrations are listed in Table 4, and

TABLE 4 Properties of Ca^{2+} oscillations under different extracellular Ca^{2+} concentrations

Ca_{Extra} (μM)	Amplitude (μM)	Frequency (Hz)	Onset (s)	Duration (s)	Potential range (mV)
0.1	0.5594	0.0030	326.1	13.65	−65.6~−60.7
1	0.6016	0.0048	195.6	14.15	−67.1~−62.2
10	0.6280	0.0060	152.5	14.54	−68.2~−63.2
100	0.6475	0.0068	132.0	14.89	−68.8~−64.1
1500	0.6614	0.0072	125.0	15.26	−70.0~−64.9

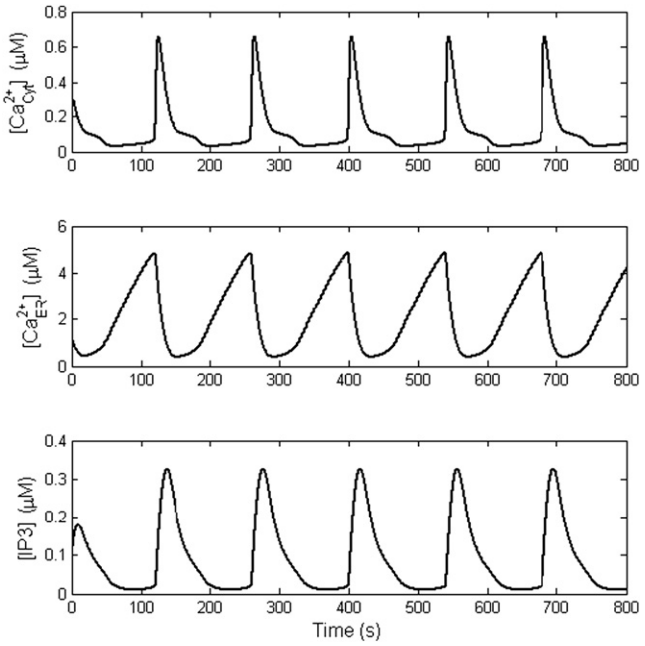

FIGURE 3 Typical spontaneous Ca^{2+} oscillations from the computational study. From top to bottom, the three plots correspond to oscillations in cytoplasmic Ca^{2+}, ER Ca^{2+}, and cytoplasmic IP_3. All three variables have the same frequency but different peak times (details are shown in Fig. 4).

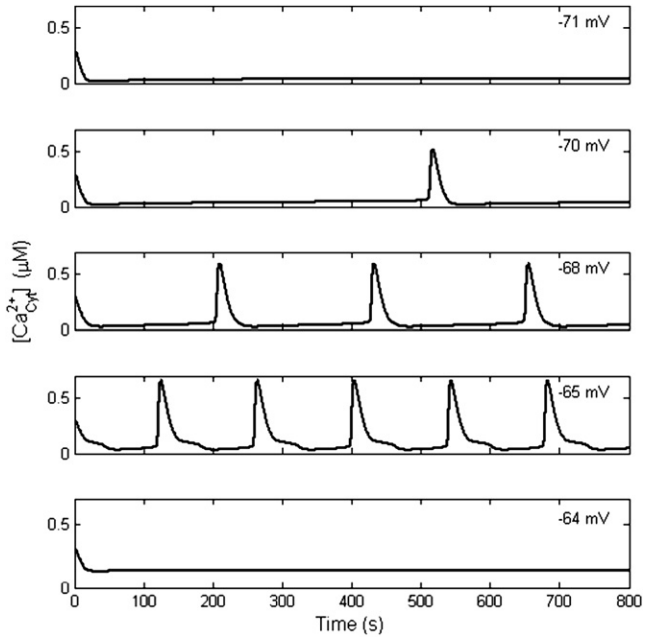

FIGURE 5 The occurrence of Ca^{2+} oscillation depends on the membrane potential. When the membrane potential is <-70.0 mV or >-64.9 mV, there is no Ca^{2+} oscillation. Within –70.0 to –64.9 mV, the frequency and amplitude of Ca^{2+} oscillations change with the membrane potential.

the values are similar to those in Table 3. Even though the extracellular Ca^{2+} concentration changed by four orders of magnitude, the amplitude and duration changed only slightly, while the frequency changed more than twofold. In fact, at different extracellular Ca^{2+} concentrations, the range of membrane potentials over which oscillations arose changed little, except for shifting to more negative resting values (Table 4). Correspondingly, the Nernst potential values of Ca^{2+} were 0 mV, 29.8 mV, 59.5 mV, 89.3 mV, and 124.2 mV. The Nernst potential of Ca^{2+} was the primary force for Ca^{2+} influx. Higher ECS Ca^{2+} concentrations, increasing the number of Ca^{2+} oscillations, reinforced the influence of extracellular Ca^{2+} influx (16).

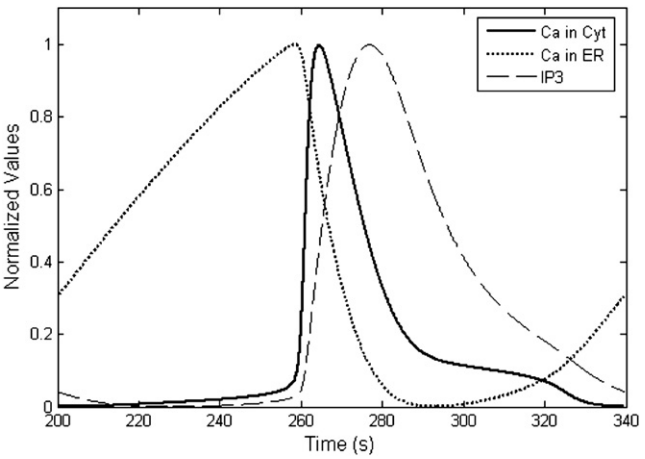

FIGURE 4 Normalized plot of the three variables in Fig. 3, during one period of Ca^{2+} oscillations. Their peak time points are ranked as ER Ca^{2+}, cytoplasmic Ca^{2+}, and cytoplasmic IP_3. Before the sudden increase in cytoplasmic Ca^{2+}, ER Ca^{2+} increased slowly.

Dependence of Ca^{2+} oscillations on temperature

By changing the temperature of the system, the features of Ca^{2+} oscillations also changed. The frequency and amplitude of Ca^{2+} oscillations are presented in Fig. 8. At a temperature between 20 and 37°C, spontaneous Ca^{2+} oscillations occurred frequently and presented a slightly higher amplitude at a low temperature. Moreover, Ca^{2+} oscillations had a longer duration at a low temperature (11,34). This point was validated from 20 to 37°C by simulation. The duration values were 15.1 s and 13.8 s at temperature points of 20 and 37°C. The characteristics were consistent with experiments (11,34). According to the Nernst equation, it was easy to establish that the increase of temperature would reduce the membrane potential. This might explain the specific dependence of Ca^{2+} oscillations on temperature.

Contribution of different VGCCs to Ca^{2+} oscillations

In our model, it was easy to test the influence on Ca^{2+} oscillations due to different VGCCs. By blocking a specific VGCC, the dependence of Ca^{2+} oscillations on VGCCs was demonstrated (Fig. 9). T- and R-types of VGCCs showed little effect on Ca^{2+} oscillations. L- and N-types of VGCCs had an effective influence on Ca^{2+} oscillations. The blocker of L-type VGCC decreased Ca^{2+} oscillations to 51.4% of control, while the blocker of N-type decreased Ca^{2+}

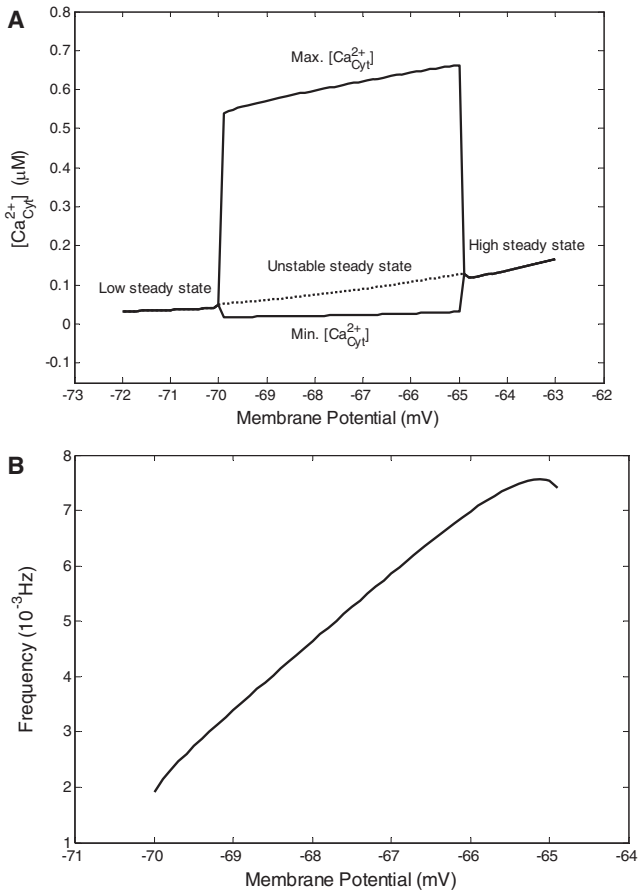

FIGURE 6 (*A*) Bifurcation diagram of Ca^{2+} oscillations as a function of membrane potential. Sustained Ca^{2+} oscillations occurred in the potential range of –70.0 to –64.9 mV, where the maximum and minimum of Ca^{2+} oscillations were plotted. The dashed line refers to the unstable steady state. Out of the oscillatory domain, the system evolved into a stable steady state. (*B*) Frequency of Ca^{2+} oscillations versus membrane potential.

oscillations only to 73.6% as was found in experiments (11). The results might relate to the different contribution on Ca^{2+} influx from different VGCCs (Fig. 10). At −65 mV, the mean influx in one period was 0.0624 μM/s, and the L-, N-, R-, and T-types contributed 59.2%, 37.0%, 2.7%, and 1.2%, respectively.

DISCUSSION

Oscillation of cytosol Ca^{2+} concentration is a ubiquitous phenomenon in a variety of cells (21,23,35). This study focused on modeling spontaneous astrocytic Ca^{2+} oscillation, which is one of the forms of astrocytic Ca^{2+} signaling defined as repetitive increases of cytosol Ca^{2+} concentration within a single cell (7). Independently of neuronal activity, spontaneous astrocytic Ca^{2+} oscillations were observed in different regions of the brain, such as cortex (14), hippocampus (36), and thalamus (11,16). Some results indicated active and direct signaling from astrocytes to neurons (11,37). Therefore, understanding the mechanisms of spontaneous astrocytic Ca^{2+} oscillations and signaling is highly important. This study successfully reproduced the oscillatory phenomenon in silico and obtained several new insights into channel dynamics dependence and frequency-encoded signaling.

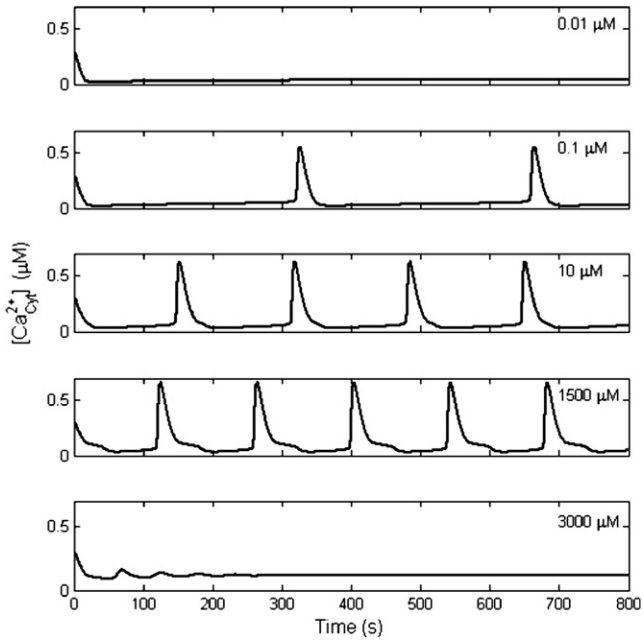

FIGURE 7 Dependence of Ca^{2+} oscillations on extracellular Ca^{2+} concentration. Ca^{2+} oscillations stopped when the extracellular Ca^{2+} concentration was too low or too high. From 0.1 to 1500 μM, the frequency of Ca^{2+} oscillations increased with a rise in extracellular Ca^{2+} concentration.

Firstly, spontaneous Ca^{2+} oscillations were found to occur at a resting membrane potential (11,16,17,36). We used −75 to −60 mV as the resting potential range for astrocytes, as suggested in the previous comprehensive review (1). Our data showed that spontaneous Ca^{2+} oscillations occurred

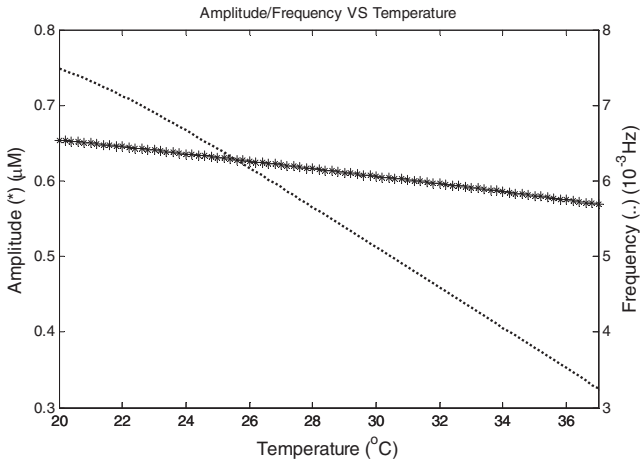

FIGURE 8 Amplitude and frequency of Ca^{2+} oscillations versus temperature. In the temperature range of 20–37°C, both the amplitude (indicated as an *asterisk*) and frequency (*dotted line*) decreased with temperature.

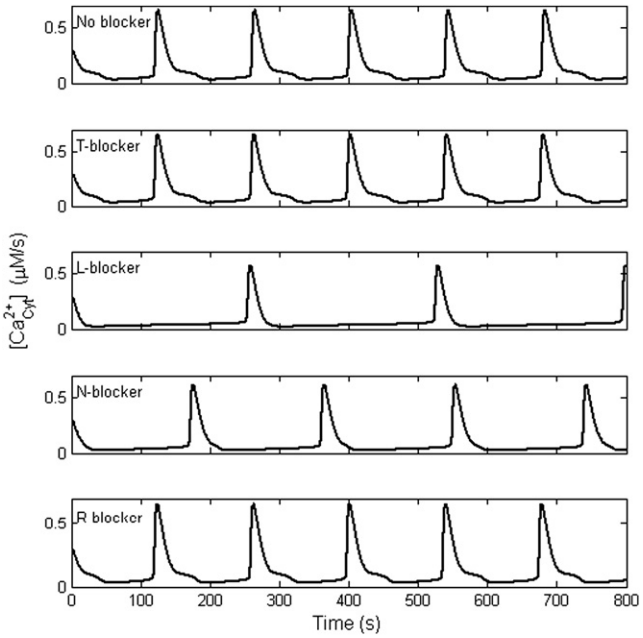

FIGURE 9 Dependence of Ca^{2+} oscillations on different VGCCs. T- and R-type of VGCCs showed little effect on Ca^{2+} oscillations. L- and N-type of VGCCs had effective influence on Ca^{2+} oscillations. Blocking the L-type VGCC decreased Ca^{2+} oscillations to 51.4% of control, while blocking the N-type decreased Ca^{2+} oscillations to 73.6%.

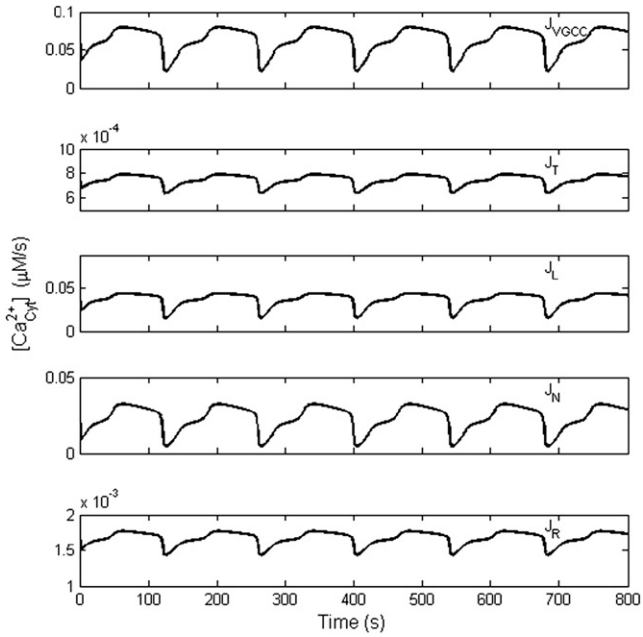

FIGURE 10 Contribution of Ca^{2+} entry through different VGCCs. All the results were obtained with the membrane potential of –65 mV. J_{VGCC} was the total flux from all the VGCCs, and J_T, J_L, J_N, and J_R indicate the partial flux through the T-, L-, N-, and R-type channel, respectively.

in the range of −70.0 to −60.7 mV (see Table 4), which might be the physiological basis for spontaneous Ca^{2+} oscillations. Recently, the resting potential of individual astrocytes was reported to vary dramatically from −85 to −25 mV (38). Naturally, this would only lead some subpopulations of astrocytes to oscillations (17). Indeed, there was a well-defined regime of membrane potential over which calcium oscillations took place (see the bifurcation diagram in Fig. 6 *A*). Around the resting potential, the T-type channel is the most reliably activated and the L-type is the least (Fig. 2). However, in this study, the steady-state conductance parameter of the L-type is much larger than that of the T-type. It was thus reasonable to find that the L-type channel contributed 59.2% of the total calcium influx for Ca^{2+} oscillation at −65 mV. On the other hand, the L-type channel was far from being fully activated, so that the total calcium influx was very small (26,39). There is a technical difficulty in assessing the small Ca^{2+} entry under the detection limit of ordinary patch systems (<1 pA/pF) (20,40).

Secondly, the dynamics of Ca^{2+} oscillations were found to relate to membrane potential, Ca^{2+} concentration in ECS, temperature, and the blocking of different VGCCs. In changing the above conditions, in our study, the frequency was ~0.0019 to 0.0072 Hz, as compared to the reported frequency between 0.003 and 0.01 Hz (11). The period of spontaneous Ca^{2+} oscillation was ~139.5 to 528.1 s, as compared to the experimental period of 98.9 to 333 s (11,14). One review suggested a common feature: spontaneous Ca^{2+} oscillations in astrocytes have a larger time-period (perhaps greater than 10-fold larger) than induced oscillations (41). The amplitude of Ca^{2+} oscillation was ~0.5276 to 0.6614 μM, in good agreement with earlier reports (26,33). The half-maximal duration of Ca^{2+} oscillations was ~13.51 to 15.26 s, which was quite similar to the observation of 15 ± 1 s in experiments (11). Generally, the amplitude and half-maximal duration changed slightly, but the frequency varied greatly. The dynamic range of the frequency in our work was ~4 (0.0072:0.0019). The amplitude change of Ca^{2+} oscillation was relatively constant (<25%), which was calculated from the values shown in Table 3 ((0.6614–0.5276):0.5276). In addition, the half-maximal duration changed within 13% ((15.26–13.51):13.51). All these properties suggest that the Ca^{2+} oscillation is likely an all-or-none process. The great change of frequency, depending on the parameters, might be relevant to the frequency-encoded signaling in astrocytes (42,43).

Thirdly, our model provided several new insights by studying the dynamic Ca^{2+} influx. In the LH model (26), the Ca^{2+} influx from the ECS to the cytosol was considered as a constant. It was easily manipulated in modeling, but was not closely related to external experimental conditions. By incorporating VGCCs into the LH model, the experimental conditions (11,16) could be easily modeled in this study. At −65 mV, the influx through different types of VGCCs and the total influx were recorded (Fig. 10). During one period, the mean influx of Ca^{2+} was 0.0624 μM/s, while the maximum and the minimum were 0.0792 and 0.0221 μM/s. All the three values were out of the range of the constant influx for sustained Ca^{2+} oscillations in the LH

model. When several mean influx values in our model were used as constant influx inputs in the LH model, the properties of Ca^{2+} oscillations from different models were divergent (details not shown). Generally, a delay of onset, a decrease in frequency (i.e., increase in period), and an increase of half-maximal duration and in amplitude were found in the LH model with the same mean influx. This suggests that the mean influx could not entirely account for the spontaneous Ca^{2+} oscillations. The properties of Ca^{2+} oscillations should be related to the dynamics of Ca^{2+} influx. This demonstrates that calcium channels dynamics cannot be disregarded when studying Ca^{2+} oscillations.

Fourthly, the main criticism of this study might be that we used a deterministic model. It could not reproduce Ca^{2+} oscillations with random spikes (44,45). As we know, some intrinsic processes during oscillation should be described as stochastic: not only is the calcium channel dynamics a random process, but so is the buffer effect of calcium influx in ICS (32,44–46). The local environmental conditions (including ions concentration, temperature, membrane potential, and pharmacological agents) of individual astrocytes should be fluctuating. In addition, VGCCs in astrocytes vary greatly in different parts of the brain, both in magnitude and type (1,29,47,48). Changing the parameters in our model could partially fill these gaps. For example, the variation of radius was found to change the spontaneous Ca^{2+} oscillations. If the density of calcium channels was taken to be constant, a smaller radius led to a higher frequency. At the median value of -70.0 to -60.7 mV, Ca^{2+} oscillations presented in the radius range from 3 to 7.5 μm. It corresponded well with the reported soma radius for astrocytes (11,14,33). Since experiments indicated that extracellular Ca^{2+} has a role in spontaneous Ca^{2+} oscillations (16,49), we tested different ECS Ca^{2+} concentrations within the concentration range of these experiments (Table 4). Neuronal activity might cause local depletion of calcium in the ECS: the change of Ca^{2+} concentration was relatively small (from 2 mM to >1 mM) and occurred in a short period of time (within 10 s) (50). We revealed that this kind of calcium depletion slightly influenced the spontaneous Ca^{2+} oscillation (results not shown). Interestingly, the interval distribution from random Ca^{2+} spikes (i.e., Ca^{2+} oscillations) in experiments demonstrated robust information transmission (44,45). This suggests the usefulness of the work presented here, in the study of frequency-encoded signaling in astrocytes.

In the future, more-applicable computational models need to be developed and tested. A central role of the IP_3-aided CICR was addressed in this study. The activation and inhibition of the IP_3 receptor showed a bell-shaped dependence described by Eq. 9 (51). However, CICR via ryanodine receptors was also suggested as a mechanism in cortical astrocytes' Ca^{2+} oscillations (14). Some experiments revealed that Ca^{2+} oscillations were independent of VGCCs (49). These studies suggested other possible mechanisms of Ca^{2+} oscillations, related to ligand-gated channels or store-operated calcium influx (9,40,52). The specific pathway for spontaneous astrocytes' Ca^{2+} oscillations needs to be clarified. In this study, ER Ca^{2+}, cytoplasmic Ca^{2+} and IP_3 oscillations with the same frequency but different peak time-points were found. This suggests that the detection of ER Ca^{2+} concentration might predict the cytoplasmic Ca^{2+} oscillation. Recently, genetically encoded fluorescent IP_3 sensors have been used to monitor the dynamics of cytosolic IP_3 during Ca^{2+} oscillation in HeLa cells: IP_3 showed a leading edge during induced Ca^{2+} oscillation (53). In this work, however, IP_3 oscillated with a peak lagging after cytoplasmic Ca^{2+} oscillation (21,22,33). Thus, experimental monitoring of IP_3 oscillations might help to elucidate the IP_3 pathway in spontaneous Ca^{2+} oscillation and determine whether the IP_3 oscillation lag is a signature of spontaneous oscillation as opposed to induced oscillation. Finally, the generation of spontaneous Ca^{2+} oscillations in different cells might not be due to one and the same mechanism, thus the complexity of Ca^{2+} oscillations emphasizes the role of computational modeling (25,26). In summary, this study provides an exploratory paradigm for simulation of spontaneous Ca^{2+} oscillations in astrocytes.

SUPPORTING MATERIAL

MATLAB codes are available at http://www.biophysj.org/biophysj/supplemental/S0006-3495(09)013824.

The authors are very grateful to Prof. A. Mayevsky, T. Obrenovitch, J. Ding, and the anonymous reviewers for their valuable comments and suggestions.

This work was supported by the National High Technology Research and Development Program of China (863 Program grant No. 2006AA02Z343), the National Natural Science Foundation of China (grants No. 60828009 and No. 30800313), and the 111 Project.

REFERENCES

1. Verkhratsky, A., R. K. Orkand, and H. Kettenmann. 1998. Glial calcium: homeostasis and signaling function. *Physiol. Rev.* 78:99–141.
2. Temburni, M. K., and M. H. Jacob. 2001. New functions for glia in the brain. *Proc. Natl. Acad. Sci. USA.* 98:3631–3632.
3. Anderson, C. M., and M. Nedergaard. 2003. Astrocyte-mediated control of cerebral microcirculation. *Trends Neurosci.* 26:340–344, author reply 344–345.
4. Takano, T., G. F. Tian, W. Peng, N. Lou, W. Libionka, et al. 2006. Astrocyte-mediated control of cerebral blood flow. *Nat. Neurosci.* 9:260–267.
5. Zonta, M., M. C. Angulo, S. Gobbo, B. Rosengarten, K. A. Hossmann, et al. 2003. Neuron-to-astrocyte signaling is central to the dynamic control of brain microcirculation. *Nat. Neurosci.* 6:43–50.
6. Kanemaru, K., Y. Okubo, K. Hirose, and M. Iino. 2007. Regulation of neurite growth by spontaneous Ca^{2+} oscillations in astrocytes. *J. Neurosci.* 27:8957–8966.
7. Nedergaard, M., B. Ransom, and S. A. Goldman. 2003. New roles for astrocytes: redefining the functional architecture of the brain. *Trends Neurosci.* 26:523–530.
8. Ransom, B., T. Behar, and M. Nedergaard. 2003. New roles for astrocytes (stars at last). *Trends Neurosci.* 26:520–522.

9. Liu, Q. S., Q. Xu, J. Kang, and M. Nedergaard. 2004. Astrocyte activation of presynaptic metabotropic glutamate receptors modulates hippocampal inhibitory synaptic transmission. *Neuron Glia Biol.* 1:307–316.
10. Nadkarni, S., P. Jung, and H. Levine. 2008. Astrocytes optimize the synaptic transmission of information. *PLOS Comput. Biol.* 4:e1000088.
11. Parri, H. R., T. M. Gould, and V. Crunelli. 2001. Spontaneous astrocytic Ca^{2+} oscillations in situ drive NMDAR-mediated neuronal excitation. *Nat. Neurosci.* 4:803–812.
12. Kang, N., J. Xu, Q. Xu, M. Nedergaard, and J. Kang. 2005. Astrocytic glutamate release-induced transient depolarization and epileptiform discharges in hippocampal CA1 pyramidal neurons. *J. Neurophysiol.* 94:4121–4130.
13. Nadkarni, S., and P. Jung. 2003. Spontaneous oscillations of dressed neurons: a new mechanism for epilepsy? *Phys. Rev. Lett.* 91:268101.
14. Tashiro, A., J. Goldberg, and R. Yuste. 2002. Calcium oscillations in neocortical astrocytes under epileptiform conditions. *J. Neurobiol.* 50:45–55.
15. Tian, G. F., H. Azmi, T. Takano, Q. Xu, W. Peng, et al. 2005. An astrocytic basis of epilepsy. *Nat. Med.* 11:973–981.
16. Parri, H. R., and V. Crunelli. 2003. The role of Ca^{2+} in the generation of spontaneous astrocytic Ca^{2+} oscillations. *Neuroscience.* 120:979–992.
17. Aguado, F., J. F. Espinosa-Parrilla, M. A. Carmona, and E. Soriano. 2002. Neuronal activity regulates correlated network properties of spontaneous calcium transients in astrocytes in situ. *J. Neurosci.* 22: 9430–9444.
18. Tanaka, M., K. Kawahara, T. Kosugi, T. Yamada, and T. Mioka. 2007. Changes in the spontaneous calcium oscillations for the development of the preconditioning-induced ischemic tolerance in neuron/astrocyte co-culture. *Neurochem. Res.* 32:988–1001.
19. Saheki, Y., S. T. Li, M. Matsushita, Y. M. Wu, W. H. Cai, et al. 2005. A new approach to inhibiting astrocytic IP_3-induced intracellular calcium increase in an astrocyte-neuron co-culture system. *Brain Res.* 1055:196–201.
20. Duffy, S., and B. A. MacVicar. 1994. Potassium-dependent calcium influx in acutely isolated hippocampal astrocytes. *Neuroscience.* 61:51–61.
21. Goldbeter, A., G. Dupont, and M. J. Berridge. 1990. Minimal model for signal-induced Ca^{2+} oscillations and for their frequency encoding through protein phosphorylation. *Proc. Natl. Acad. Sci. USA.* 87:1461–1465.
22. Young, G. W. D., and J. Keizer. 1992. A single-pool inositol 1,4, 5-trisphosphate-receptor-based model for agonist-stimulated oscillations in Ca^{2+} concentration. *Proc. Natl. Acad. Sci. USA.* 89:9895–9899.
23. Dupont, G., and A. Goldbeter. 1993. One-pool model for Ca^{2+} oscillations involving Ca^{2+} and inositol 1,4,5-trisphosphate as co-agonists for Ca^{2+} release. *Cell Calcium.* 14:311–322.
24. Chen, X. F., C. X. Li, P. Y. Wang, M. Li, and W. C. Wang. 2008. Dynamic simulation of the effect of calcium-release activated calcium channel on cytoplasmic Ca^{2+} oscillation. *Biophys. Chem.* 136:87–95.
25. Schuster, S., M. Marhl, and T. Hofer. 2002. Modeling of simple and complex calcium oscillations from single-cell responses to intercellular signaling. *Eur. J. Biochem. FEBS.* 269:1333–1355.
26. Lavrentovich, M., and S. Hemkin. 2008. A mathematical model of spontaneous calcium oscillations in astrocytes. *J. Theor. Biol.* 251: 553–560.
27. Rozi, A., and Y. Jia. 2003. A theoretical study of effects of cytosolic Ca^{2+} oscillations on activation of glycogen phosphorylase. *Biophys. Chem.* 106:193–202.
28. Hodgkin, A. L., and A. F. Huxley. 1952. A quantitative description of membrane current and its application to conduction and excitation in nerve. *J. Physiol.* 117:500–544.
29. Verkhratsky, A., and C. Steinhauser. 2000. Ion channels in glial cells. *Brain Res. Brain Res. Rev.* 32:380–412.
30. D'Ascenzo, M., M. Vairano, C. Andreassi, P. Navarra, G. B. Azzena, et al. 2004. Electrophysiological and molecular evidence of L-(Cav1), N- (Cav2.2), and R- (Cav2.3) type Ca^{2+} channels in rat cortical astrocytes. *Glia.* 45:354–363.
31. Amini, B., J. W. Clark, Jr., and C. C. Canavier. 1999. Calcium dynamics underlying pacemaker-like and burst firing oscillations in midbrain dopaminergic neurons: a computational study. *J. Neurophysiol.* 82:2249–2261.
32. Ullah, G., and P. Jung. 2006. Modeling the statistics of elementary calcium release events. *Biophys. J.* 90:3485–3495.
33. Ullah, G., P. Jung, and A. H. Cornell-Bell. 2006. Anti-phase calcium oscillations in astrocytes via inositol (1, 4, 5)-trisphosphate regeneration. *Cell Calcium.* 39:197–208.
34. Schipke, C. G., A. Heidemann, A. Skupin, O. Peters, M. Falcke, et al. 2008. Temperature and nitric oxide control spontaneous calcium transients in astrocytes. *Cell Calcium.* 43:285–295.
35. Goldbeter, A. 2002. Computational approaches to cellular rhythms. *Nature.* 420:238–245.
36. Nett, W. J., S. H. Oloff, and K. D. McCarthy. 2002. Hippocampal astrocytes in situ exhibit calcium oscillations that occur independent of neuronal activity. *J. Neurophysiol.* 87:528–537.
37. Nedergaard, M. 1994. Direct signaling from astrocytes to neurons in cultures of mammalian brain cells. *Science.* 263:1768–1771.
38. Bolton, S., K. Greenwood, N. Hamilton, and A. M. Butt. 2006. Regulation of the astrocyte resting membrane potential by cyclic AMP and protein kinase A. *Glia.* 54:316–328.
39. Hofer, T., L. Venance, and C. Giaume. 2002. Control and plasticity of intercellular calcium waves in astrocytes: a modeling approach. *J. Neurosci.* 22:4850–4859.
40. Putney, J. W., and G. S. Bird. 2008. Cytoplasmic calcium oscillations and store-operated calcium influx. *J. Physiol.* 586:3055–3059.
41. Montana, V., E. B. Malarkey, C. Verderio, M. Matteoli, and V. Parpura. 2006. Vesicular transmitter release from astrocytes. *Glia.* 54:700–715.
42. Pasti, L., A. Volterra, T. Pozzan, and G. Carmignoto. 1997. Intracellular calcium oscillations in astrocytes: a highly plastic, bidirectional form of communication between neurons and astrocytes in situ. *J. Neurosci.* 17:7817–7830.
43. Pasti, L., M. Zonta, T. Pozzan, S. Vicini, and G. Carmignoto. 2001. Cytosolic calcium oscillations in astrocytes may regulate exocytotic release of glutamate. *J. Neurosci.* 21:477–484.
44. Skupin, A., and M. Falcke. 2007. Statistical properties and information content of calcium oscillations. *Gen. Informat.* 18:44–53.
45. Skupin, A., H. Kettenmann, U. Winkler, M. Wartenberg, H. Sauer, et al. 2008. How does intracellular Ca^{2+} oscillate: by chance or by the clock? *Biophys. J.* 94:2404–2411.
46. Shuai, J. W., and P. Jung. 2002. Stochastic properties of Ca^{2+} release of inositol 1,4,5-trisphosphate receptor clusters. *Biophys. J.* 83:87–97.
47. Sontheimer, H. 1994. Voltage-dependent ion channels in glial cells. *Glia.* 11:156–172.
48. Sontheimer, H. 1992. Astrocytes, as well as neurons, express a diversity of ion channels. *Can. J. Physiol. Pharmacol.* 70 (Suppl.):S223–S238.
49. Wang, T. F., C. Zhou, A. H. Tang, S. Q. Wang, and Z. Chai. 2006. Cellular mechanism for spontaneous calcium oscillations in astrocytes. *Acta Pharmacol. Sin.* 27:861–868.
50. Cohen, J. E., and R. D. Fields. 2004. Extracellular calcium depletion in synaptic transmission. *Neuroscientist.* 10:12–17.
51. Falcke, M. 2004. Reading the patterns in living cells—the physics of Ca^{2+} signaling. *Adv. Phys.* 53:255–440.
52. Liu, Q. S., Q. Xu, G. Arcuino, J. Kang, and M. Nedergaard. 2004. Astrocyte-mediated activation of neuronal kainate receptors. *Proc. Natl. Acad. Sci. USA.* 101:3172–3177.
53. Matsu-ura, T., T. Michikawa, T. Inoue, A. Miyawaki, M. Yoshida, et al. 2006. Cytosolic inositol 1,4,5-trisphosphate dynamics during intracellular calcium oscillations in living cells. *J. Cell Biol.* 173:755–765.